Chapter 5
Gradual SEP Events

Abstract Gradual solar energetic-particle (SEP) events are the "big proton events" of the past and are usually much more "gradual" in their decay than in their onset. As their intensities increase, particles streaming away from the shock can amplify Alfvén waves that scatter subsequent particles, eventually limiting their flow at the "streaming limit." Waves generated by higher-speed protons running ahead can also throttle the flow of lower-energy ions, flattening spectra and altering abundances in the biggest SEP events. Yet, we find that the A/Q-dependent scattering causes abundance patterns, varying in space and time, which determine source-plasma temperatures, since the pattern of Q values of the ions depends upon temperature. Different source-plasma temperatures explain much of the variation in element abundances in gradual SEP events. In nearly 70% of gradual events, SEPs are shock-accelerated from ambient coronal plasma of ~0.8–1.6 MK, while 24% of the events involve accelerated material from active-region temperatures of 2–4 MK and include residual impulsive-suprathermal ions with pre-enhanced abundances. Non-thermal variations of the ions in gradual SEP events from 2–4 MK source plasma are greatly reduced, relative to those in impulsive SEPs, from similar plasma, probably because the accelerating shock waves average over impulsive-suprathermal ions from multiple jet sources. Later, SEPs become trapped in a *reservoir* behind the CME in gradual events, where spectra are uniform in space and decrease adiabatically in time as the magnetic bottle containing them slowly expands.

We begin by showing proton intensities in the classic large gradual SEP event of 4 November 2001 in Fig. 5.1. This event, from a source longitude of W17 on the Sun, has the typical time profile of a centrally located event (see Sect. 2.3.3). The figure lists phases of the event along the abscissa which we will study, in approximate time order, although onsets were discussed previously in Sect. 3.1.

In impulsive SEP events, most particles traveled to us scatter free so we had little need to discuss transport. With increased intensities, particles from gradual SEP events generate or amplify their own spectrum of Alfvén waves for pitch-angle scattering, which complicates their transport more and more as intensities increase. In fact, it is the resonant waves, generated by the out-flowing particles, which scatter subsequent particles back and forth across the shock, incrementally increasing acceleration that drives particles to higher and higher energy.

D.V. Reames, *Solar Energetic Particles*, Lecture Notes in Physics 932,
DOI 10.1007/978-3-319-50871-9_5

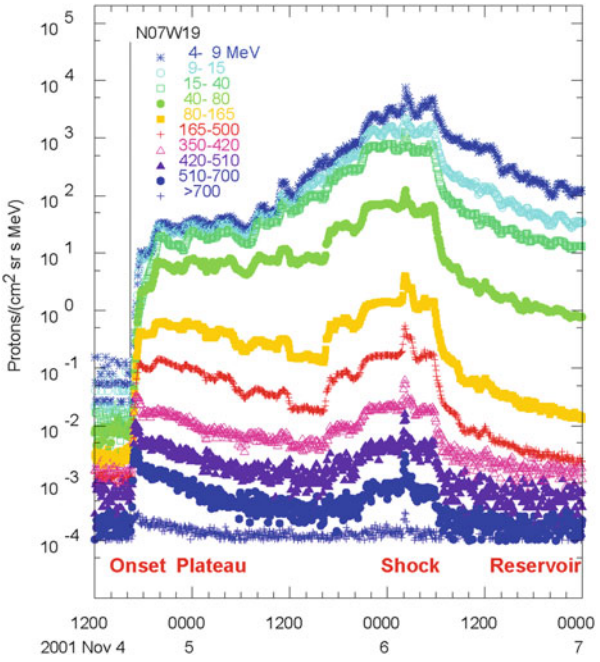

Fig. 5.1 Proton intensities vs. time from the NOAA/GOES satellite are shown for the large gradual SEP event of 4 November 2001. Distinctive event phases are listed along the abscissa (Reames 2013)

For recent reviews of gradual SEP events see Desai and Giacalone (2016) and Lee et al. (2012). For theoretical background see Parker (1963).

5.1 Parallel Transport

5.1.1 Diffusive Transport

The diffusion of particles of type X and velocity v by pitch-angle scattering with scattering mean free path λ_X with a power-law dependence on radial position r as $\lambda_0\, r^{\beta}$ varies as (Parker 1963; see Equation C1 in Ng et al. 2003)

$$n_x(r,t) = \frac{1}{4\pi\Gamma(\varepsilon)}\left(\frac{\varepsilon}{3}\right)^{2\varepsilon-1}\left(\frac{3}{\lambda_0 v t}\right)^{\varepsilon}\exp\left[\frac{-3\,r^{(2-\beta)}}{(2-\beta)^2\lambda_0 v t}\right] \tag{5.1}$$

where $\varepsilon = 3/(2-\beta)$ and β must be less than 2.

If we examine the ratio of species X and Y, where λ is a power of rigidity and where $L = \lambda_X/\lambda_Y = R^{\alpha} = ((A_X/Q_X)/(A_Y/Q_Y))^{\alpha}$, as a result of the rigidity dependence of λ, and $\tau = 3r^{2-\beta}/[\lambda_Y\,(2-\beta)^2\,v]$, it can easily be shown (e.g. Reames 2016a, b) that

$$\mathrm{X/Y} = L^{-\varepsilon}\exp[(1-1/L)\tau/t] \approx L^{\tau/t-\varepsilon} \tag{5.2}$$

The ratio in Eq. 5.2 is the enhancement or suppression relative to the ratio at the SEP source and does not include any pre-enhanced impulsive suprathermal ions, although those are also power-law in form. Thus, relative abundances vary approximately as *a power of A/Q*. This will prove to be important in determining source-plasma temperatures (Sect. 5.6). If the ratio $R > 1$, as for Fe/O, the abundance ratio, X/Y begins at infinity and falls asymptotically to $R^{-\alpha\varepsilon}$. Ratios begin at infinity because diffusion does not account for the particle transit time at the onset. Breneman and Stone (1985) observed that abundance enhancements were power laws in A/Q, rising with A/Q in some SEP events and falling in others as we saw in Fig. 2.4 in Sect. 2.4.1. In standard diffusion theory, scattering does *not* change with time; thus, the waves affect the particles, but the particles have no affect on the waves (defying energy conservation).

5.1.2 Wave Growth

The amplification of Alfvén waves by streaming protons has been discussed in textbooks on plasma physics for many years (e.g. Stix 1962, 1992; Melrose 1980; see also Ng et al. 2003; Rice et al. 2003; Li et al. 2005). In quasi-linear theory, ions, streaming along $\boldsymbol{B}$, resonate with Alfvén waves of wave number k:

$$k = \frac{B}{\mu P} \tag{5.3}$$

in the rest frame of the waves. Here $P = pc/Qe$ is the rigidity of a particle of charge Qe, and momentum p, and μ is the cosine of its pitch angle relative to $\boldsymbol{B}$.

Equation 5.3 results from quasi-linear theory (QLT) where particles are assumed to orbit the unperturbed field and the electric field vector of the circularly-polarized Alfvén wave rotates so as to maintain its phase relative to the direction of rotation of the gyrating particle. This resonance maximizes the transfer of energy between the wave and the particle, seen as pitch-angle scattering in the rest frame of the wave, or wave frame, approximately the plasma rest frame.

The growth rate of the σ polarization mode of Alfvén waves (see Ng et al. 2003; Stix 1992; Melrose 1980) produced by protons is clearest and simplest in the wave frame, where it is given by

$$\gamma_\sigma(k) = 2\pi^2 g_\sigma e^3 c V_A \iint d\mu dP \frac{P^3}{W^2} R^\sigma_{\mu\mu} \frac{\partial f_H^\pm}{\partial \mu} \tag{5.4}$$

where $g_\sigma = \pm 1$ for outward (inward) wave direction and $f_{\mathrm{H}}{}^{\pm}$ is the proton phase-space density in each corresponding wave frame. Here W is the total proton energy, and $R^\sigma{}_{\mu\mu}$ is the resonance function (see Ng and Reames 1995; Ng et al. 2003) that

imposes the resonance condition (Eq. 5.3) while allowing for resonance broadening near $\mu \approx 0$. If we can ignore the effects of slow propagation of the waves, then the wave intensity of the σ mode, $I_\sigma(k,r,t)$ obeys the simple equation

$$\frac{\partial I_\sigma(k,r,t)}{\partial t} = \gamma_\sigma(k,r,t) I_\sigma(k,r,t) \tag{5.5}$$

also in the wave frame, where we have explicitly shown the dependence upon space r and time t, which may be quite significant. We will see that the pitch-angle diffusion coefficient for protons depends linearly upon the intensity of resonant waves (Sect. 5.1.3). Equation 5.5 was used by Ng and Reames (1994) to study time-dependent wave growth during proton transport that was quantitatively consistent with the streaming limit as we will see in Sect. 5.1.5.

Thus, streaming protons grow the waves, and then the waves scatter the subsequent protons to reduce the streaming and the wave growth. This causes the scattering mean free paths to vary in both time and space (Ng et al. 2003). While the wave growth caused by heavier ions is negligible, they respond to the waves in ways that are not always obvious, a priori. Waves, grown by protons at a particular value of μP, connect to other energies and other species with the same value of μP, as shown in Eq. 5.3.

Wave growth is commonly combined with quasi-parallel shock acceleration, where scattering is especially important. However, wave growth is entirely a transport phenomenon, its dependence upon the particles is only through $\partial f_{\mathrm{H}}^{\pm}/\partial\mu$; it is otherwise completely independent of the nature of the proton source. Wave growth will also be important near quasi-perpendicular shocks when streaming intensities of protons become large. This point is sometimes overlooked by students.

Working in the wave frame is illustrative but inconvenient when both inward and outward waves are present and when the Alfvén speed V_{A} decreases as r^{-1} with distance. Transforming to the plasma frame introduces terms of order $(V_{SW} + g_\sigma V_{\mathrm{A}})/v$ (see e.g. Ng et al. 2003).

5.1.3 *Particle Transport*

The equation of particle transport may be simplified in the fixed inertial frame where f is the phase space density of a given particle species averaged over gyrophase (Roelof 1969; Ng and Reames 1994; Ng et al. 1999)

$$\frac{\partial f}{\partial t} + \mu v \frac{\partial f}{\partial r} + \frac{1-\mu^2}{r} v \frac{\partial f}{\partial \mu} - \frac{\partial}{\partial \mu}\left(D_{\mu\mu}\frac{\partial f}{\partial \mu}\right) = G \tag{5.6}$$

The third term in Eq. 5.6 represents focusing of the particles in the diverging magnetic field while the fourth term represents pitch-angle scattering with the diffusion coefficient $D_{\mu\mu}$. Here v is the particle speed, μ is its pitch angle, and the term G on the

right-hand side of the equation represents particle sources, for example, it might be a power-law energy spectrum times a delta-function at the radial location of a shock wave.

The diffusion coefficient $D_{\mu\mu}$ is given by

$$D_{\mu\mu} = \frac{v^2}{4P^2} \sum_{\sigma} \int dk I_{\sigma} R^{\sigma}_{\mu\mu} \tag{5.7}$$

where P is the particle rigidity and σ runs over wave modes. The wave intensity I_{σ} and the resonance function $R^{\sigma}{}_{\mu\mu}$ were discussed in the previous section.

The set of Eqs. 5.4–5.7 completely describe the evolution of both particles and waves and their coupling together. Equation 5.4 shows that the growth of waves is controlled by the streaming particles and Eq. 5.7 relates the particle scattering to the intensity of waves. Scattering causes wave growth as a direct consequence of energy conservation (Ng et al. 2003, Appendix 2).

5.1.4 Initial Abundance Ratios

We noted above that in diffusion theory, when λ has a power-law dependence on rigidity, hence upon A/Q, ratios like Fe/O or He/H begin with large enhancements that decrease with time. While this occurs for small gradual SEP events, Fig. 5.2 shows that He/H can reverse in large SEP events where wave growth becomes important. This is an example of a case where the arrival of protons depends upon their own velocity, but their affect on He, for example, depends upon protons of a higher velocity, and their common value of μP.

Why does the initial behavior reverse for He/H in the large event? The early ions stream out into space from the event with $\mu \approx 1$ with few resonant Alfvén waves and little scattering. The H at 2 MeV, for example, suffers little scattering and is only beginning to make its own resonant waves. The He at 2 MeV amu^{-1}, however, is scattered by waves that were amplified by 8-MeV protons (same rigidity) that came out much earlier. If the intensity of 8-MeV protons is high (i.e. a big event), they arrive earlier and generate waves so the 2-MeV amu^{-1} He will be scattered much more than the 2-MeV H. Similar logic applies to He/H at higher energies. This effect does not occur for Fe/O since both species are scattered by earlier proton-generated waves. Also, waves that scatter Fe are coupled to protons of quite high energy, which are less intense, so they actually increase Fe/O initially. The progression of enhancements is modeled by Ng et al. (2003).

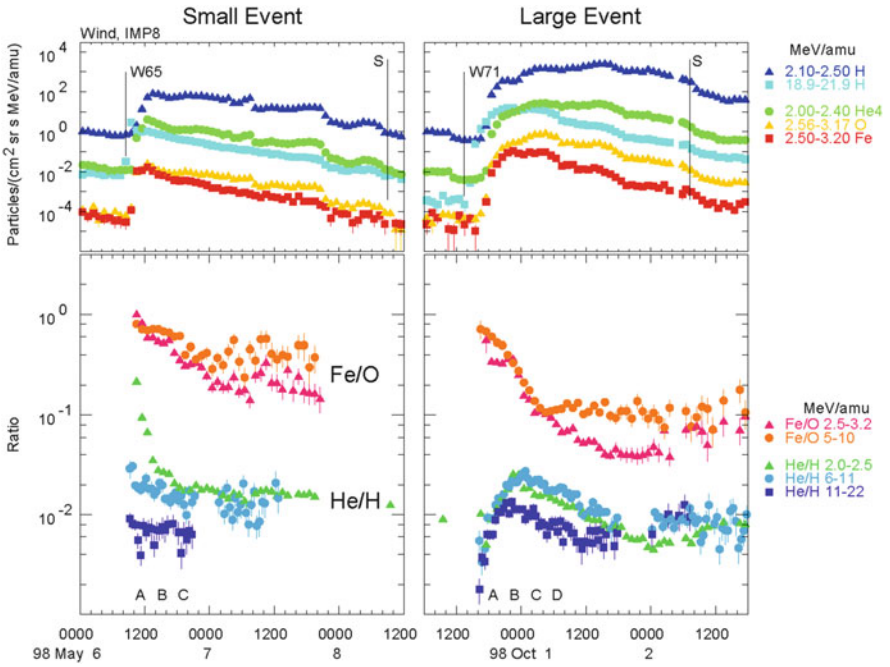

Fig. 5.2 Particle intensities and abundance ratios are shown for small (*left*) and large (*right*) gradual SEP events (Reames et al. 2000). Proton spectra at A, B, C, and D, shown in the reference, are much more intense in the October event

5.1.5 The Streaming Limit

In a study of large SEP events observed at the *Helios* spacecraft in solar orbit, Reames (1990) noticed that there was an early plateau period (see Fig. 5.1) during large SEP events near 1 AU, where the proton intensities seemed to have an upper limit of intensities as shown in Fig. 5.3.

The intensities can rise much higher at the shock peaks, which are the particle source, because particles at the shock have no net streaming. The streaming limit is a transport phenomenon.

Imagine an experiment that slowly increases the SEP injection intensity at a source near the Sun. At first, the intensity at 1 AU would increase proportionally. Then, at higher source intensities, wave growth would begin to scatter and trap the particles, with most wave growth near the source where intensities are highest. Eventually, further increasing flow from the source would increase the wave growth and scattering so much that the intensity at 1 AU would no longer increase. This is the "streaming limit" that also emerges from theoretical transport models that include wave growth (e.g. Lee 1983, 2005; Ng and Reames 1994; Ng et al. 2003, 2012). The intensity behavior at 1 AU vs. that at the source near the Sun is shown in the left panel of Fig. 5.4 while the

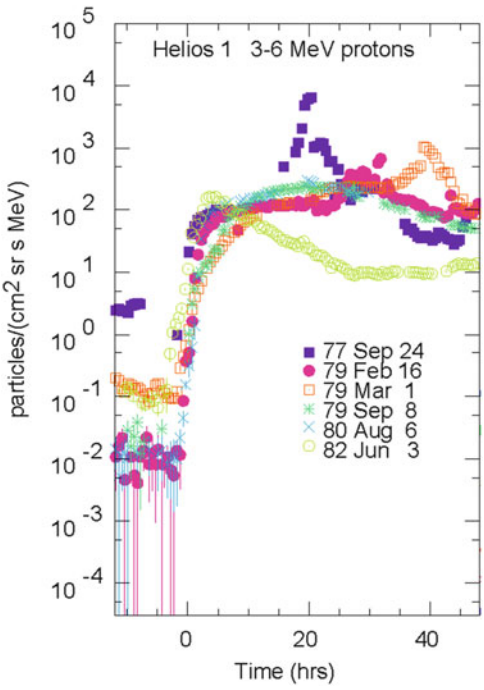

Fig. 5.3 Initial intensities of 3–6 MeV protons are shown overlapped for six large SEP events, all near 1 AU. Intensities do not seem to exceed ~200 $(cm^2\ sr\ s\ MeV)^{-1}$ early in the events, but can become much higher later when shock peaks arrive (Reames 1990)

right panel shows the spatial dependence caused by increasing injection levels at the source.

Note that the wave growth depends upon the *absolute* value of the streaming intensity and the parameters shown in Eq. 5.4; there are *no arbitrarily adjustable parameters*. The peak intensity in the left panel of Fig. 5.4 is just over 200 $(cm^2\ sr\ s\ MeV)^{-1}$, similar to the value observed in Fig. 5.3.

However, the plateau intensities in the largest gradual SEP events can involve more than just waves that are self-generated by particles of a single energy. They can involve waves generated by higher-energy protons that contribute to the scattering of lower-energy ions by coupling through the μ dependence of Eq. 5.3. These waves preferentially retard the low-energy particles and flatten the power-law source spectra on the plateau as seen in the left panel of Fig. 5.5. Intense protons of 10–100 MeV stream out early, generating waves as they scatter toward smaller μ. Waves generated at high P and low μ resonate with ions of low P and $\mu \approx 1$ which are coming behind more slowly. Thus, waves amplified by protons of 10 MeV at $\mu \approx 0.5$ will scatter ions at 2.5 MeV amu^{-1} and $\mu \approx 1$, retarding their flow and thus flattening their spectrum at 1 AU.

Some proof of this mechanism in given by its absence in the 2 May 1998 SEP event; its plateau proton spectrum is shown in the right panel of Fig. 5.5. The spectrum in this event remains a power law since the intensity of 10 MeV protons is two orders of magnitude smaller than that in 28 October 2003. The low intensities of 10–100 MeV protons do not generate enough waves to suppress the low-energy spectrum in the May

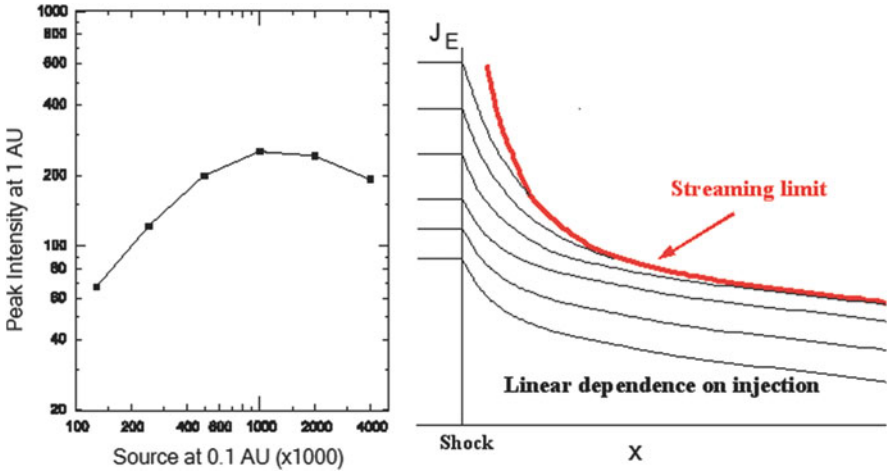

Fig. 5.4 The *left panel* shows intensity at 1 AU vs. that at 0.1 AU. The *right panel* shows the spatial variation as the source intensity level is increased with linear behavior at low intensities (see Ng and Reames 1994; Ng et al. 2003, 2012)

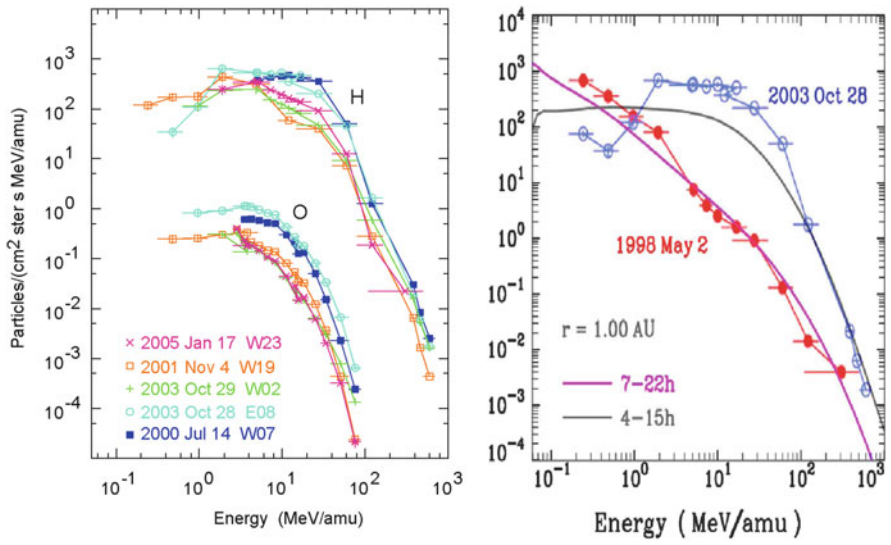

Fig. 5.5 The *left panel* shows energy spectra of H and O in five large gradual SEP events (all GLEs) that are flattened at low energies (Reames and Ng 2010). The *right panel* shows that the small event of 2 May 1998, with greatly reduced H intensities at 10–100 MeV, cannot generate enough waves to suppress lower energies. Model fits to the spectra are shown in *grey* and *purple* (Ng et al. 2012)

event. The theoretical fits to these spectra, shown in Fig. 5.5, support this explanation. Wave growth can control spectral shape.

5.1.6 Electron Transport

Non-relativistic electrons cannot resonate with Alfvén waves, so they do not participate in much of the physics we have just described. Low-energy electrons usually propagate scatter free with highly-anisotropic angular distributions mainly because of absorption by the solar wind of 0.1–1 Hz frequencies that would resonate with the electrons. Electron spectra often show a break in the ~100-keV energy region. Above the break the spectrum steepens and the width of the angular distribution broadens as scattering becomes much more important (see Tan et al. 2011). It is sometimes erroneously concluded that 1 MeV electrons are accelerated much later than those at 20–50 keV in SEP events; this apparent delay could result from transport rather than acceleration.

5.2 Angular Distributions

Angular distributions also show the effects of increased scattering when high proton intensities amplify waves. This is seen in the angular distributions of H and He ions in large and small SEP events as shown in Fig. 5.6. The particle intensities remain clustered along the field direction around 180° for more than a day in the angular distributions in the small event on the left in Fig. 5.6 but, in the more intense event on the right, the angular distributions begin to spread in only a few hours.

Of course, the scattering and the wave growth depend upon the initial wave intensity. However, small impulsive and gradual events usually remain scatter-free and angular distributions rapidly isotropize in more-intense gradual events and especially in GLEs (see Reames et al. 2001). Most SEP events begin nearly scatter free at energies above a few MeV amu^{-1}, but not at low energies where μ-coupling shown in Fig. 5.5 applies and traps ions with energies below a few MeV amu^{-1} near their source.

5.3 Models and Shock Acceleration

General information about shock formation and acceleration may be found in comprehensive review articles (Jones and Ellison 1991; Lee et al. 2012). However, there is such compelling experimental evidence of wave growth in the larger gradual SEPs events that we focus on models that include it.

The earliest time-equilibrium model of shock acceleration with self-consistent treatment of particles and waves was the work of Bell (1978a, b) on GCRs, which was subsequently adapted to interplanetary shocks by Lee (1983). Shock models

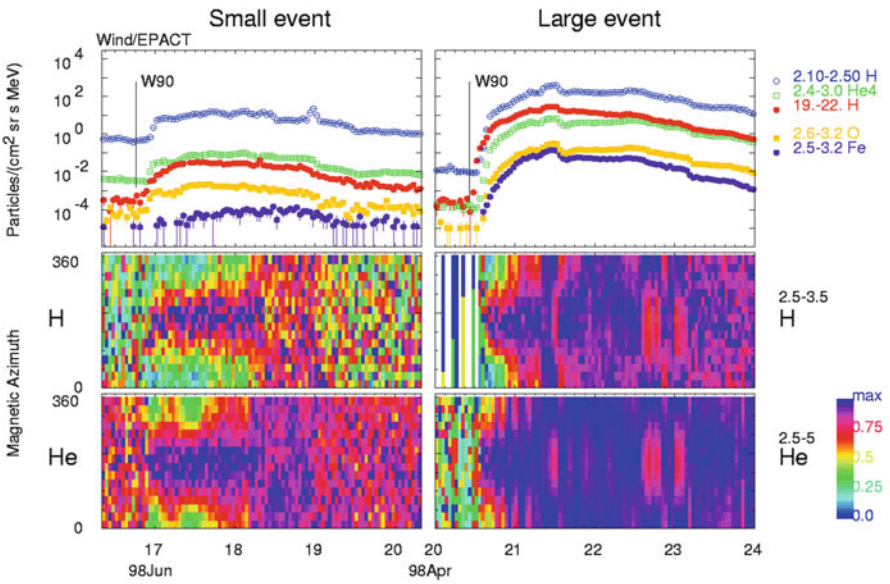

Fig. 5.6 Intensities (*top*) and angular distributions, relative to $\boldsymbol{B}$, for H (*middle*) and ^{4}He (*bottom*) are shown for large (*left*) and small (*right*) gradual SEP events. Note the much higher intensity of the (*red*) 19–22 MeV protons in the *upper right panel*

were applied to acceleration of GeV protons in the corona by Zank et al. (2000, see also Lee 2005; Sandroos and Vainio 2007; Zank et al. 2007; Afanasiev et al. 2016).

The time-dependent self-consistent model of particle transport with wave amplification (Ng et al. 2003) was applied to shock acceleration by Ng and Reames (2008) resulting in modeling of the time-evolution of the proton spectra at the shock shown in Fig. 5.7 along with the evolution of the radial dependence of the intensity upstream of the shock for a given energy proton. A streaming limit soon forms within 0.1 R_S of the shock as seen in the right panel.

An interesting feature of the time-dependent numerical acceleration calculations is the growth of waves as the proton spectrum grows to higher energy. With the growth of waves that resonate with particles of the highest energy E_1 and rigidity P_1, some protons will begin to be accelerated to still-higher energy E_2 and rigidity P_2. Initially, the only waves that can trap ions at E_2 are those that resonate with protons with $\mu_2 < P_1/P_2$, i.e. only at small μ_2 can ions at the new energy find resonant waves generated by lower-energy protons. Thus at each new energy the particles begin with a pancake distribution at small μ (Ng and Reames 2008).

The Ng and Reames (2008) model prevents the scattering from approaching the Bohm limit by requiring that the scattering mean free path be more than three times the particle gyroradius, so that the quasi-linear approximation remains valid. This makes the maximum energy lower and the acceleration rate slower than that in the calculation of Zank et al. (2000), who assumed the more-likely Bohm limit where scattering mean free path equals the particle gyroradius, i.e. $\delta B/B \approx 1$, as has been observed in strong

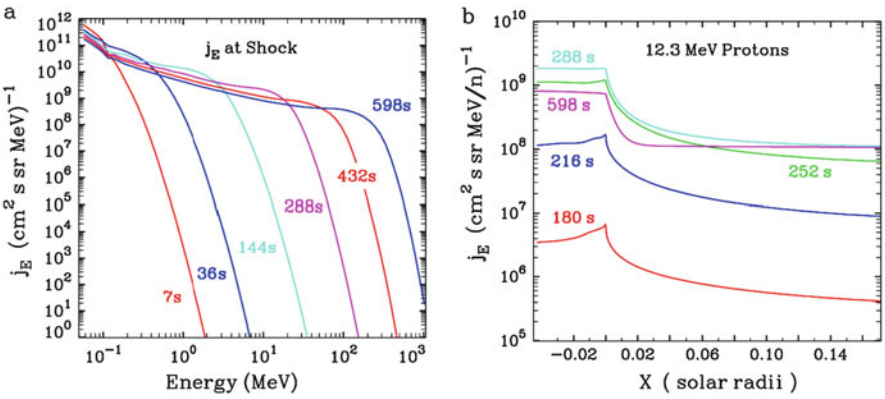

Fig. 5.7 The *left panel* (***a***) shows the time evolution of the proton energy spectrum at the shock for the first ~10 min. The *right panel* (***b***) shows the time evolution of the spatial distribution of 12.3 MeV protons upstream of the shock. Once accelerated at ~3 min, 12.3 MeV proton intensities increase to form a streaming limit within 0.1 R_S of the shock at ~4.2 min (Ng and Reames 2008)

shocks (Lario and Decker 2002; Terasawa et al. 2006). It is also true that an oblique shock, where ions gain energy in the $\mathbf{V_S} \times \boldsymbol{B}$ electric field, can affect the acceleration time and maximum energy by increasing the particle energy gained on each traversal of the shock. We would speculate that a fast shock traversing a sufficiently dense seed population should have no trouble accelerating GeV protons in a few minutes or even less.

It can not escape our attention that it is much easier for theoreticians to work in a universe where particle scattering in constant in time, and waves never grow. Quasi-perpendicular shocks need no change in scattering to increase acceleration, only a small change in θ_{Bn}. Such approximations are often useful in making tractable solutions to explore specific functional dependences. However, observations show that wave growth dominates the largest SEP events. Further realistic studies that include it could help advance our understanding of these important events.

5.4 Shock Acceleration In Situ

Traveling interplanetary shock waves near Earth are the local continuation of the CME-driven shock waves that produce gradual SEP events. These shocks provide an opportunity to directly measure, in situ, the properties of accelerated particles together with the characteristics of the shock and its driver under an extremely wide variety of shock conditions (see e.g. Berdichevsky et al. 2000). Desai et al. (2003) showed that low-energy ion abundances near the shock peak were much more closely related to ambient abundances of those ions upstream of the shock than to the abundances of the corresponding elements in the solar wind, as might be expected from our discussion of the seed population in Sect. 2.4.3. Desai et al. (2004) found that energy spectra at the shocks

were better correlated with the spectra upstream than with those expected from the shock compression ratio. Especially for low-energy ions, shock acceleration persists far out from the Sun and tends to reaccelerate ions from the same population that was accelerated earlier.

The choice of a location to measure the ambient, background, or reference abundances and spectra upstream of the shock is difficult. If it is chosen prior to the time that shock leaves the Sun, perhaps ~2–3 days before the shock arrival, then solar rotation insures that background is sampled at a longitude of 26°–40° to the west of the longitude sampled at the shock peak. If it is chosen hours prior to the shock arrival, background will be dominated by particles accelerated earlier by the same shock. Neither choice is ideal.

In effect, the re-acceleration of ions from the seed population found in the reservoir of an earlier event evokes the classical two-shock problem considered, for example, in the review by Axford (1981) and more recently by Melrose and Pope (1993). Here, the integral equilibrium distribution function $f(p)$ of momentum p of accelerated particles from a shock with compression ratio s is

$$f_a(p) = ap^{-a} \int_0^p dq\, q^{a-1} \phi(\mathrm{q}) \tag{5.8}$$

where $a = 3s/(s-1)$ and $\phi(p)$ is the injected distribution. If we take $\phi(p)$ as a delta function at p_0 we find a power-law spectrum $f_a(p) \sim (p/p_0)^{-a}$ after the first shock. If we reapply Eq. 5.8, injecting $f_a(p)$ into a shock with compression ratio s' and let $b = 3s'/(s'-1)$, we find that integrating the power law gives

$$f_{a,b}(p) = \frac{kab}{p_0(b-a)} \left[\left(\frac{p}{p_0} \right)^{-a} - \left(\frac{p}{p_0} \right)^{-b} \right] \quad \text{for} \quad a \neq b. \tag{5.9}$$

The corresponding intensity is $j(E) = p^2 f(p)$.

Note that Eq. 5.9 is symmetric in the powers a and b, and will be dominated by the shape of the hardest, flattest spectrum, either the background (i.e. a) or the new shock, b. Thus, it is no surprise that one finds local-shock spectra that are dominated by the shape of the upstream background spectrum (Desai et al. 2004; Reames 2012) produced earlier when the shock was stronger. A further complication occurs when we include a spectral knee with a factor like $\exp(-E/E_0)$ (e.g. Ellison and Ramaty 1985; see also Mewaldt et al. 2012) to allow for the finite acceleration time. At energies above the knee, observers will find spectra that are much steeper than either the background or the expected equilibrium spectra.

These possibilities for spectral shapes were considered in the observations of Reames (2012), who studied ^{4}He spectra of ~1–10 MeV amu^{-1} in 258 in situ interplanetary shocks observed by the *Wind* spacecraft. The purpose of this study was to determine which shock parameters were important to produce measurable particle acceleration and which were not. Figure 5.8 shows a well-defined shock event, shock number 83.

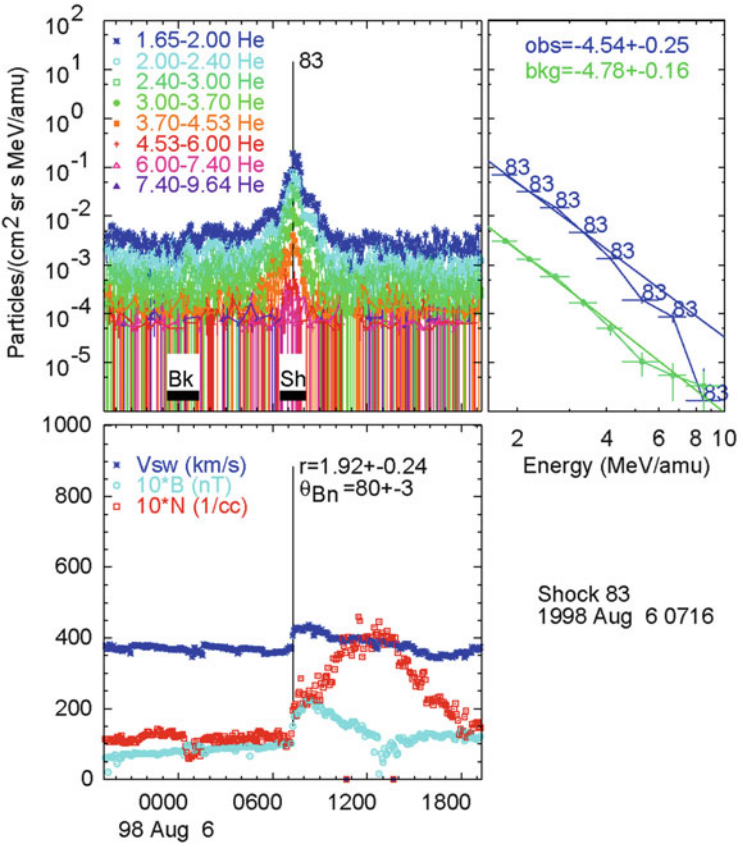

Fig. 5.8 Particle intensities are shown vs. time in the *upper left panel* with plasma parameters below for shock number 83. Spectra of the shock and background are shown to the *right* with spectral slopes indicated

Particle intensities in Fig. 5.8 are shown in the upper left panel, the plasma parameters: solar-wind speed V_{SW}, magnetic field B, and density N, in the lower left panel, and the shock and background spectra in the upper right panel. The times over which the two spectra are taken are shown in the upper left panel (Bk and Sh). This is a quasi-perpendicular shock with the angle between B and the shock normal, $\theta_{Bn} = 80° \pm 3°$.

Figure 5.9 compares properties of the shocks in this study. The left panel shows a histogram of the shock speed distribution for all of the shocks and for the subset that showed measurable particle acceleration. High shock speed was the strongest determinant for measurable acceleration, followed by high shock compression ratio, and large θ_{Bn}. High background intensity was also important; more input produced more output. Measurable acceleration was more than twice as likely for shocks with $\theta_{Bn} > 60°$ as for those with $\theta_{Bn} < 60°$. Quasi-parallel shocks, i.e. small θ_{Bn}, may have been more likely to have knee energies below the energy of observation. Recently, Zank et al.

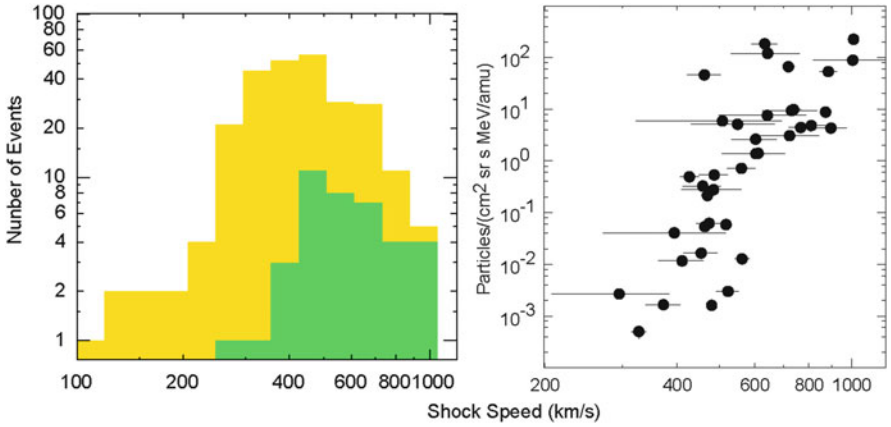

Fig. 5.9 The *left panel* shows the distribution of shock waves at 1 AU with measurable acceleration of >1 MeV amu^{-1} ^{4}He vs. shock speed (*green*) within the distribution of all 258 shock waves vs. shock speed (*yellow* and *green*) observed by the *Wind* spacecraft. The *right panel* shows the background-corrected peak intensity of 1.6–2.0 MeV amu^{-1} ^{4}He vs. shock speed for the shocks in situ. Shock speed is the strongest determinant of accelerated intensity for local shocks; this mirrors the correlated behavior of peak intensity vs. CME speed in Fig. 2.11 (adapted from Reames 2012, 2013)

(2006) have suggested that "higher proton energies are achieved at quasi-parallel rather than highly perpendicular interplanetary shocks within 1 AU." The in situ observations (Reames 2012) show the opposite; quasi-perpendicular shocks are favored; this difference may occur because ample pre-accelerated seed populations were available for the real shocks.

The right panel in Fig. 5.9 shows the background-corrected peak shock intensity of 1.6–2.0 MeV amu^{-1} ^{4}He as a function of shock speed. The shock speed has a correlation coefficient of 0.80 with intensity. This correlation for in situ shocks mirrors the correlation of peak proton intensity with CME speed in Fig. 2.11 as modified by Rouillard et al. (2012) and shown in the lower right-hand panel of Fig. 3.4.

Particle intensities peak at the time of shock passage in nearly all of the events in the Reames (2012) study. However, sometimes intensities peak before or after shock passage when a spacecraft encounters magnetic flux tubes that connect it to a stronger part of the shock nearby, perhaps even one with a different value of θ_{Bn}.

Absolute intensities of accelerated particles are not directly predicted by acceleration theories that omit wave growth. The rate of injection of seed particles is treated as an adjustable parameter—more input results in more output, and this is the case for in situ events. However, streaming protons and increasing wave intensities can trap particles near the source. At a few powerful shock waves, such as 20 October 1989, it has been observed that the energy in energetic particles exceeds that in the plasma and magnetic field (Lario and Decker 2002). Those authors suggested that the peak intensities of particles up to 500 MeV are simply trapped in a region of low density and low magnetic field near a shock. Maybe, but, how did they get there? Surely they

were accelerated there. Perhaps the wave-trapped particles are in the process of destroying (i.e. pushing apart B at) the shock that accelerated them. Another shock where the particle energy exceeds the magnetic energy is that of 6 November 2001, in Fig. 5.1 (C. K. Ng, private communication), where the sharp proton peak up to 700 MeV shows a shock that is still clearly intact. This is the issue of "cosmic-ray-mediated" shocks discussed by Terasawa et al. (2006) for two additional interplanetary shocks. This is a fascinating process that can be observed, in situ, at some interplanetary shocks.

5.5 Abundances and FIP

We began by discussing the reference abundances in Chap. 1 and comparing them with the solar photospheric abundances as a function of first ionization potential (FIP) in Fig. 1.6. The reference abundances are obtained by averaging over many gradual SEP events. Since the transport of particles varies as a power of A/Q (see Eq. 5.2), different species such as Fe and O will be distributed differently in space and time, but these particles are conserved. If we can successfully average over time or space we will recover the source abundances. If this assumption is correct and our averaging is representative, the reference abundances will approach the coronal abundances. Evidence for the space-time distribution is shown in Fig. 5.10.

The SEP event on the East flank of the CME (W85 source, on the left in Fig. 5.10), shows enhancement of Fe/O early then suppression later, since Fe, with higher A/Q, scatters less than O. Ne/O, involving similar values of A/Q, varies little. Solar rotation and the Parker spiral translates this time variation into a spatial one and the events toward the West flank of the CME show mainly depleted Fe/O.

5.6 Source-Plasma Temperatures

Since particle transport in gradual SEPs varies as a power of A/Q, and Q varies with T, we can use this power law to find the source-plasma temperature T that gives the best-fit pattern of A/Q, just as we did for impulsive events. Figure 5.11 (similar to Fig. 4.8) shows A/Q vs. T with Q derived from the atomic physics.

The red shaded region in Fig. 5.11 is 2.5–3.2 MK, corresponding to active region temperatures that we found for the impulsive SEP events (see Sect. 4.6). As we decrease T below this region, O, then N, then C move from the 0-electron to the 2-electron closed shells. Meanwhile, Ca, then Ar, then S, then Si, then Mg move from the 2-electron to the 8-electron shells. Thus, we can tell the temperature by the pattern of abundance enhancements. We need only notice which elements are in which group; which elements have no enhancement like He; which elements are in the group with Ne; which are in the group with Ar.

Figure 5.12 compares the observed pattern of enhancements early in a large gradual SEP event (on the left) with the pattern of A/Q (on the right). The patterns match best

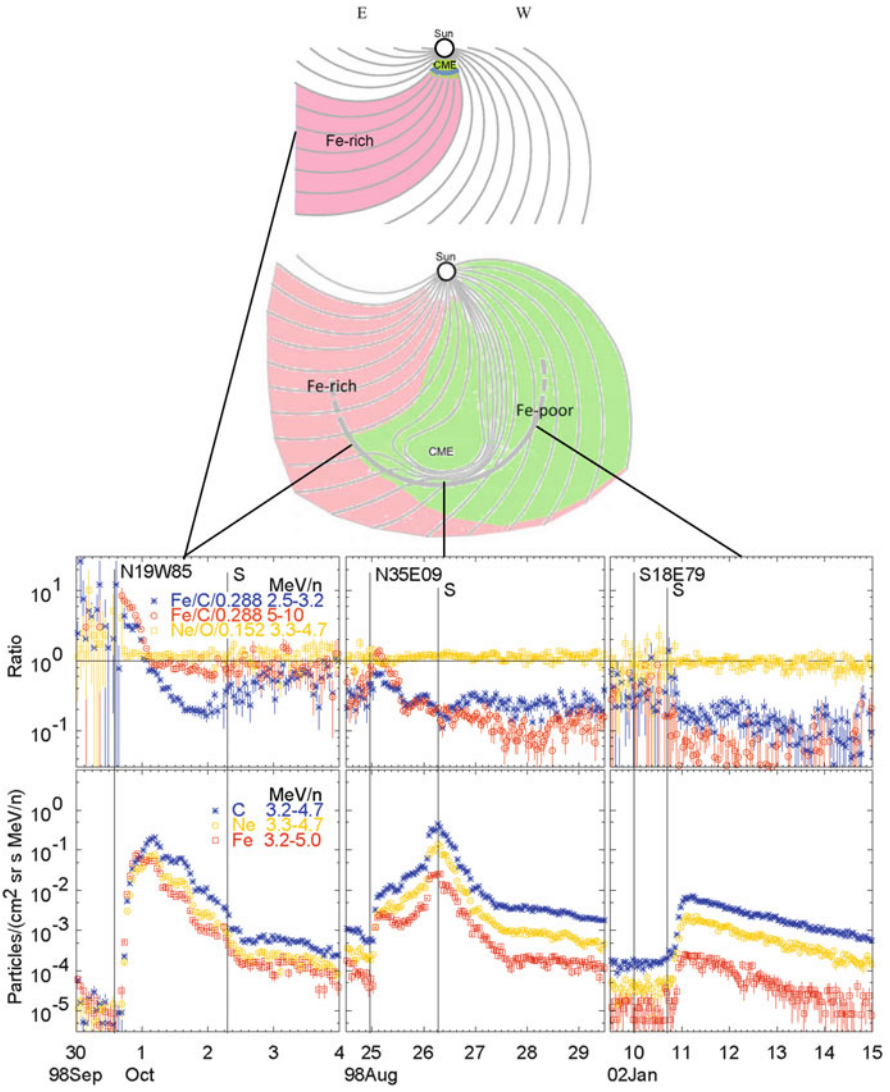

Fig. 5.10 Intensities of C, Ne, and Fe are shown for three gradual SEP events at different solar longitudes in the *lower panels*, relative abundances in the *middle panels*, and the location and evolution of a CME above (after Reames 2014)

near $T \approx 0.6$ MK, an unusually low temperature for SEP events. Note that C, N, and O have moved well above He to the 2-electron shell with Ne, while Mg, Si, and S have moved up to the 8-electron shell close to Ar and Ca. Patterns of enhancement in other SEP events are shown in Reames (2016a).

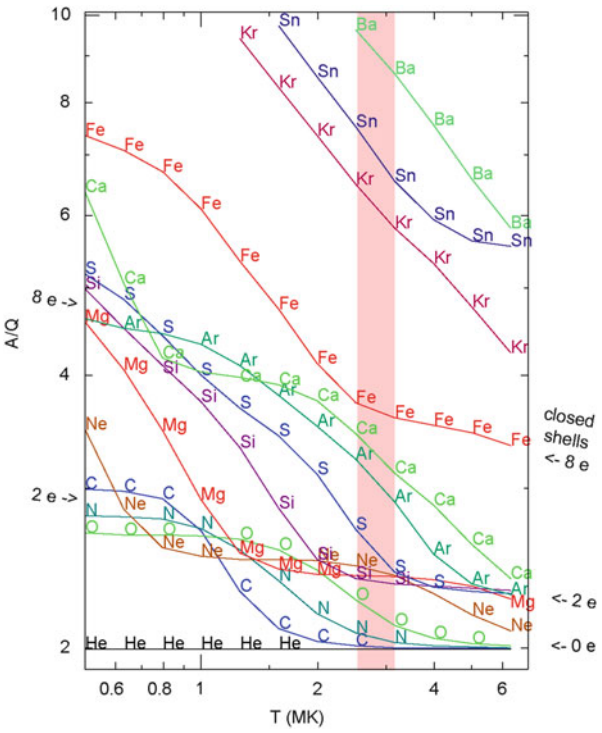

Fig. 5.11 A/Q is plotted as a function of the theoretical equilibrium temperature for the elements named along each curve. Points are spaced 0.1 units of $\log_{10} T$ from 5.7 to 6.8. Bands produced by closed electron shells with 0, 2, and 8 orbital electrons are indicated, He having no electrons at this T. Elements tend to move from one closed-shell group to another as the temperature changes. (Data for $Z \leq 28$ from Mazzotta et al. 1998, for $Z > 28$ from Post et al. 1977)

For the LEMT telescope on the *Wind* spacecraft, 8-h intervals during a large SEP event will provide adequate statistics for the rarer elements to determine enhancement patterns. For each 8-h period we can calculate least-squares fits of enhancement vs. $A/Q(T)$ for all values of T in the range of interest and plot χ^2 of the fit vs. T (upper-right panel in Fig. 5.13). The minimum value of χ^2 gives the best-fit temperature and power of A/Q for that time. This process gives the source-plasma temperature as a function of time during an event, as shown in the upper-left panel of Fig. 5.13 for the event of 8 November 2000. For this event we find temperatures near 1 MK for all time periods with either abundance enhancements or suppressions. For two of the time periods, the best fits to enhancement vs. A/Q are shown in the lower-right panel of Fig. 5.13. However, for time periods when enhancements in the abundances are flat, neither enhanced nor suppressed, we cannot measure T, since any A/Q values will fit and χ^2 has no minimum. Larger enhancement or suppression of the abundances produces clearer minima in χ^2 and smaller errors in T.

For 45 gradual SEP events that had reasonably well-defined temperatures, Reames (2016a) found:

- 69% (31 events) showed ambient coronal temperatures $T \leq 1.6$ MK
- 24% (11 events) had $2.5 \leq T \leq 3.2$ MK active region temperatures, like impulsive SEP events

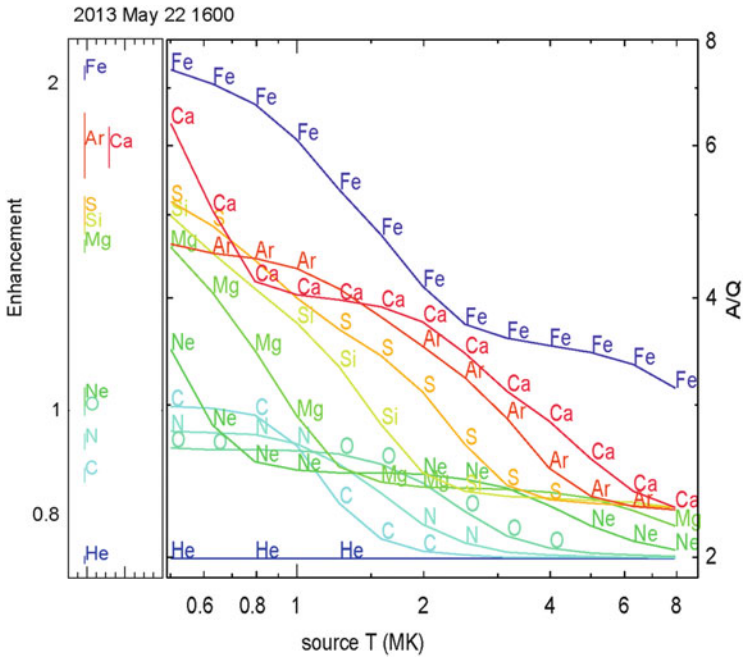

Fig. 5.12 The left panel shows the abundance enhancements at ~3–5 MeV amu^{-1} observed early in the 22 May 2013 SEP event. The right panel compares a section of the A/Q vs. T plot from Fig. 5.11. The patterns match at about 0.6 MK (Reames 2016a)

Some (11) of the events with ambient coronal temperatures showed a second minimum at the upper limit of T in χ^2 vs. T. These probably represent a component of ions that have been stripped by passing residual impulsive suprathermal ions through a small amount of material before reacceleration by the shock.

While the gradual event temperatures and fit parameters are not strongly correlated with any particular properties of the accelerating CME or shock, Fig. 5.14 shows T vs. CME speed. The un-weighted correlation coefficient is -0.49 for these events. Events that happen to be GLEs are identified in the figure; their temperature distribution and other properties are similar to those of the other gradual SEP events.

We now realize that attempts to study abundance cross-correlations in gradual SEP events were ineffective because most variations were caused by temperature differences that previously were not known. For example the average value of Fe/O is a factor of ~10 higher in gradual events with $T = 3.2$ MK than in those with $T = 1.5$ MK. This is shown in Fig. 5.15 which plots normalized Fe/O vs. C/He, for intervals during the gradual SEP events, in both panels, with T as symbols in the lower panel and power of A/Q as symbols in the upper.

The area of abundances showing active-region temperatures $T \geq 2$ MK is immediately distinguishable, clustering in the upper left of the lower panel of Fig. 5.15. These events are distinguished as open circles in the upper panel as well. Points during events accelerated from specific temperatures of ambient coronal plasma stretch from

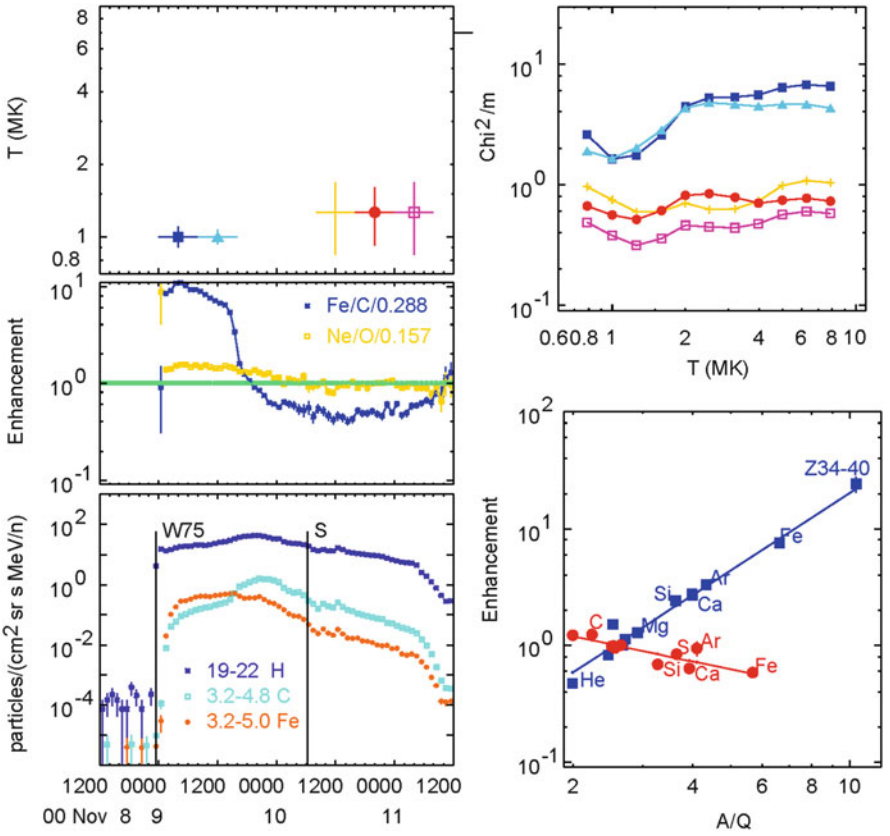

Fig. 5.13 Clockwise from the *lower-left panel* are the intensities of H, C, and Fe during the 8 November 2000 SEP event, the enhancements in Fe and Ne during the event, the best-fit temperatures in color-coded 8-h intervals, values of χ^2/m vs. T for each time interval (where m is the number of degrees of freedom), and two sample fits of enhancements, relative to O, vs. A/Q (Reames 2016a)

upper right, with steep A/Q enhancements early in the events, toward the lower center, where the A/Q slopes are reduced or negative, late in the events.

One might well ask: why do we use theoretical values of Q vs. T when there are actually some measurements of Q (e.g. DiFabio et al. 2008)? Mainly, Q_{Fe} for example, measured at 1 AU, is observed to increase with energy at low energies, suggesting that the ions have traversed enough material after acceleration to strip them to equilibrium charges that depend upon their velocity, especially in these impulsive events. The theoretical charges are more likely to be appropriate earlier, i.e. at the time of acceleration. In addition, the theoretical charges from atomic physics are available for essentially all elements we measure.

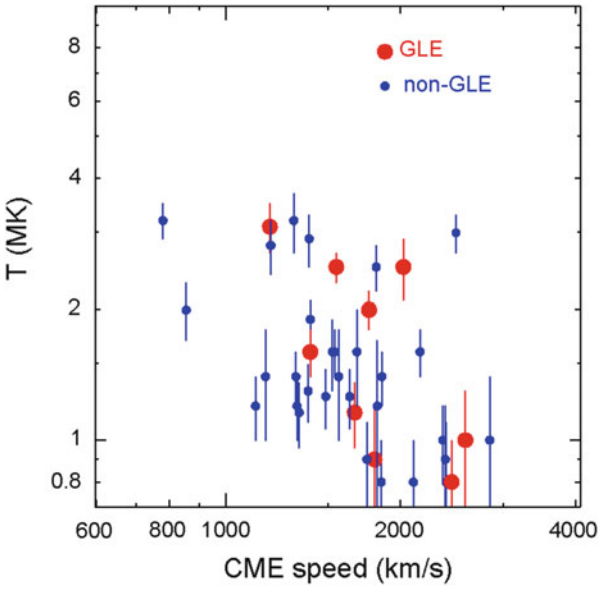

Fig. 5.14 Source-plasma temperature is shown as a function of associated CME speed for gradual SEP events with GLE events identified (data from Reames 2016a)

5.7 Spatial Distributions and the Reservoir

As spacecraft began to probe more-distant areas of the heliosphere, it became possible to view spatial distributions of SEPs, and their time variations, within a single SEP event. While spatial gradients were expected, it was rather surprising that equal intensities of ~20 MeV protons were found over long distances of solar longitude of ~180° on the *Pioneer* spacecraft by McKibben (1972). Twenty years later equal intensities were found late in large events over 2.5 AU between *Ulysses* and IMP 8 near Earth by Roelof et al. (1992) who named the regions "reservoirs." Reservoirs extend to *Ulysses* at heliolatitudes up to >70°, N and S (Lario 2010), and they are also seen in other electron observations (Daibog et al. 2003).

The *Helios* mission provided another opportunity to measure the evolution of SEP events at different longitudes confirming that the longitude distribution of Fig. 2.1 was appropriate for each individual event. Figure 5.16 shows that, at widely separated spacecraft, the intensities merge with that at *Helios 1* as each spacecraft joins it in the reservoir. Spectra are identical throughout the reservoir but decrease adiabatically with time as the volume of this "magnetic bottle" expands. (The drawing in the lower panel of Fig. 5.16 shows the spacecraft penetrating the CME; in reality, of course, the spacecraft are nearly stationary as the CME expands past them, but that version would be much more difficult to draw.)

If there were significant leakage from the reservoir, one would expect the highest-energy protons to leak first, since they are faster, scatter less, and encounter the boundary most often, but this would steepen the spectrum with time and is *not* observed. Thus the leakage is minimal.

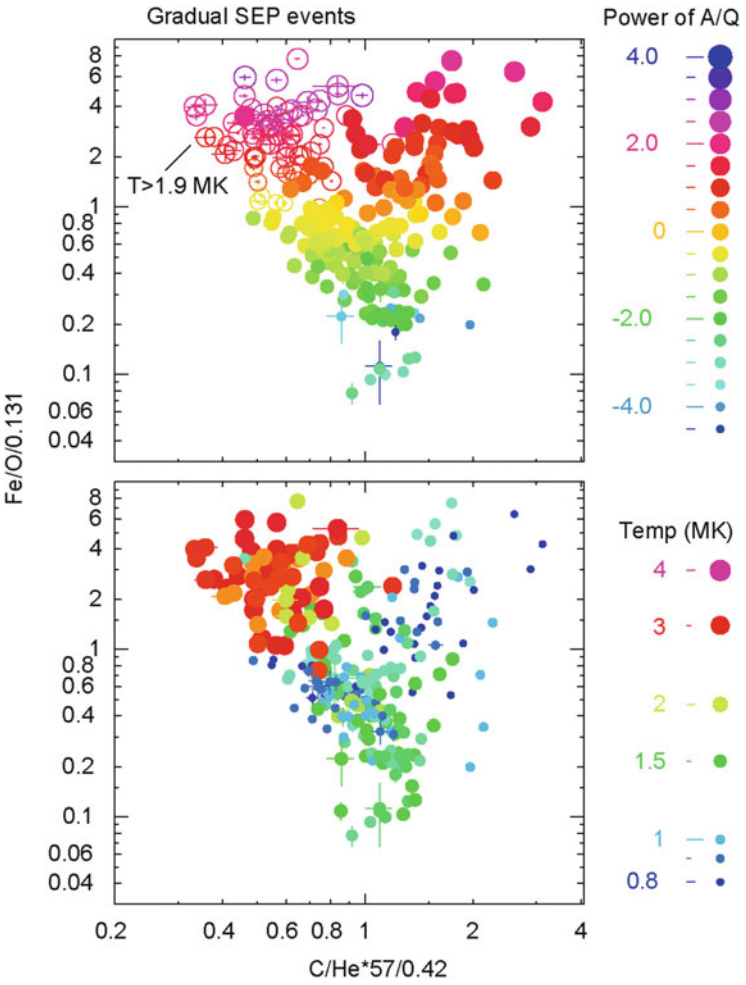

Fig. 5.15 Normalized abundance ratios Fe/O vs. He/C is plotted in both panels with symbol size and color representing T (*lower panel*) and power of A/Q (*upper panel*) (Reames 2016b)

One common, but rather poor, way of comparing spatial variations is to plot peak intensity at, say three, spacecraft vs. longitude and fit the three points with a parabola. Does this measure particle spread in longitude? Suppose we made such a plot with the data shown in Fig. 5.16. The intensity at *Helios 1* peaks at the time of shock passage. The intensity at *Helios 2* peaks when it enters the reservoir, where it has the same intensity as *Helios 1*. The intensity at IMP 8 peaks when it enters the reservoir later, where *all three intensities are equal*. What does the parabola defined by these three peak intensities measure? Is it the spread of the particles or the spread in the trapping volume behind the CME with time? The peaks all occur at different times and that *essential* timing information is lost when plotting only peak intensities vs. longitude.

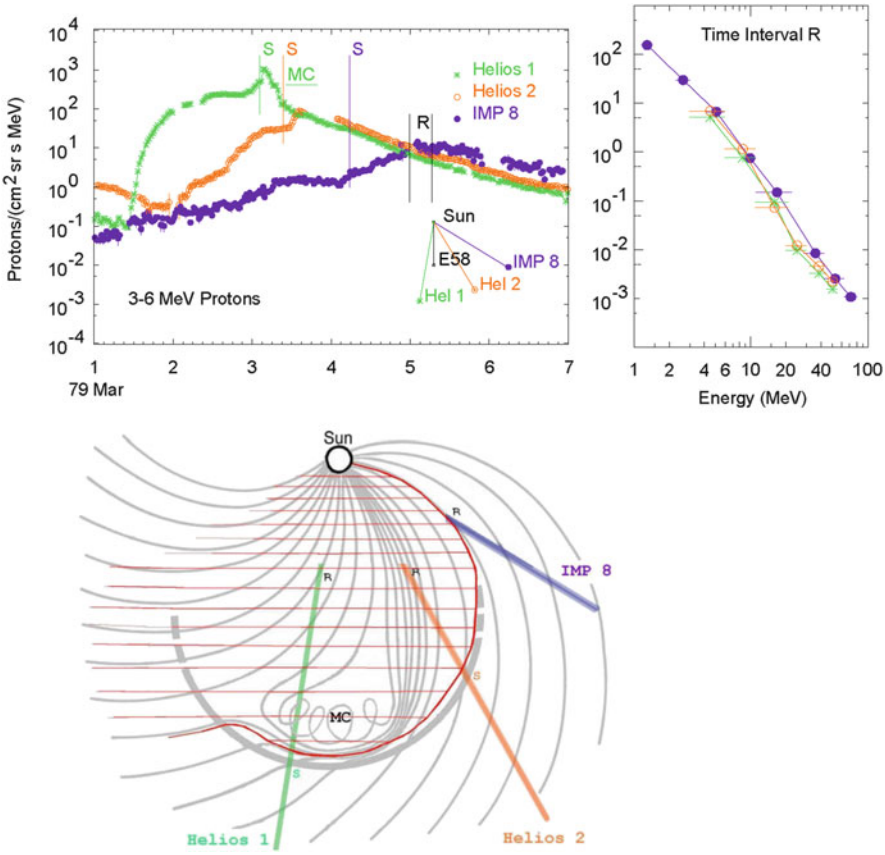

Fig. 5.16 The *upper left panel* shows the intensities of 3–6 MeV protons at three spacecraft vs. time. The paths of the spacecraft into the expanding CME are shown below as they penetrate into the reservoir region (*red hashing*) behind the shock and CME where all intensities and spectra (*upper right*) are equal spatially, though they decrease with time as the trapping volume expands (Reames 2013; after Reames et al. 1997b)

Isn't it more important to note that all intensities are equal when the intensity at IMP 8 peaks? It seems more productive to try to *distinguish* spatial and temporal effects rather than combining them.

For a single spacecraft, one way to show that spectra do not change their shape in time is to normalize the intensity-vs.-time plots at one point in time. If they stay normalized subsequently, then the spectral shapes are invariant. This is shown for two gradual SEP events in Fig. 5.17. This technique demonstrates invariance even when the spectra do not have power-law form. Multiple spacecraft at different locations can be included or abundance variations can be compared similarly.

Note that the reservoir can extend upstream of the CME and shock on the East flank, as seen in the *left panel* of Fig. 5.17; here the particles may be partly contained by self-amplified waves from earlier streaming or by preexisting magnetic boundaries.

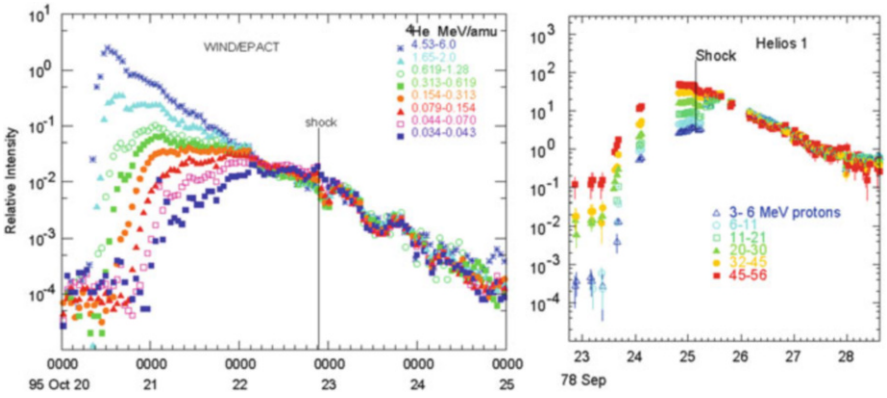

Fig. 5.17 In invariant spectral regions, particle intensities at different energies maintain the same relative normalization as a function of time, as shown for different species in two different events (Reames 2013; after Reames et al. 1997a, b)

The realization that the slow decline in a gradual SEP event results from expansion of a reservoir is most important because it displaces the previous idea that slow particle diffusion explained the decay phase of events. Actually, reservoirs are scatter free, as shown by the striking example from Mason et al. (1989) shown as Fig. 2.2 in Sect. 2.3.4. A whole literature of fitting SEP events to diffusion theory had emerged, leading to the "Palmer (1982) consensus" that "$\lambda_{\parallel} = 0.08$–$0.3$ AU over a wide range of rigidity." This is yet another example of the misapplication of diffusion theory; the intensity decline comes from the expansion of a magnetic bottle in time, not inefficient transport through space. There are no significant spatial gradients within reservoirs.

It is important to recognize that reservoirs trap energetic ions in an expanding volume above the solar surface for a long period of time. While this population of particles tends to be mirrored in the converging magnetic fields above the corona, some undoubtedly scatter into the loss cone and plunge into the corona to produce γ-rays (just as the particles in flaring loops must do). Vestrand and Forrest (1993) observed γ-ray production spanning over ≈30° of the Sun's surface in the large GLE of 29 September 1989. Also, Ryan (2000) discussed long-duration γ-ray events lasting an hour or more while the flare-associated X-rays died away rapidly. See, also, the recent long-duration γ-ray observations by Ackermann et al. (2014) and Ajello et al. (2014). Reservoirs provide an invariant spectrum of shock-accelerated ions that can bombard a large area of the solar corona with slowly decreasing SEP intensities for hours or days.

5.8 Non-thermal Variations: Impulsive Vs. Gradual SEPs

Knowing the source-plasma temperatures allows us to compare impulsive and gradual SEP events from the same temperature source—e.g. from active regions. Figure 5.18 compares the normalized abundances of O/C vs. C/He for impulsive and gradual SEP events plotted at the same scale. The impulsive events have been limited to those with

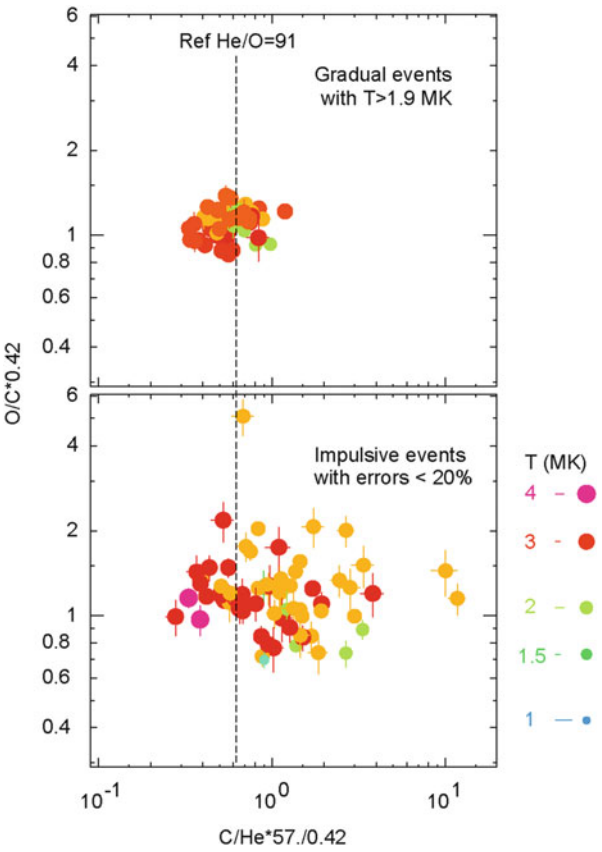

Fig. 5.18 Enhancements of O/C vs. C/He are compared, for gradual events with $T \geq 2.0$ MK (*upper panel*) and impulsive events with <20% errors (*lower panel*). Both panels are plotted at the same scale and T is indicated by the size and color of the symbols. (1) The distribution is much smaller for the gradual events. (2) The median of the distribution of C/He for the gradual events, shown as a *dashed line*, implies a reference value for He/O of 91 rather than 57 (Reames 2016b)

modest <20% statistical errors in the ratios and the gradual events come from active region plasma at $T \geq 2$ MK.

Especially at a temperature of 3.2 MK (red symbols in Fig. 5.18) the elements He and C are likely to be fully ionized and O is nearly so (as seen in Fig. 5.11). Thus the ratios should be unaltered source abundances for both populations. However the dashed line also shows that the normalization is wrong for C/He since the central mean should be at 1.0. This suggests that the reference abundance He/O should be 91 rather than 57. This would bring He in somewhat better alignment with other high-FIP elements on a FIP plot (Fig. 1.6) and is shown as a red open circle on that figure.

More significantly, the spread in the distribution of gradual events is much smaller than that of impulsive events in Fig. 5.18. The spread in the impulsive events must come from non-thermal abundance variations in the local plasma where reconnection is occurring. However, neither wave-particle interactions nor magnetic reconnection can alter C/He when both elements have $A/Q = 2.0$. If the shock of a gradual SEP event were accelerating only suprathermal ions from a single impulsive source, we would expect the same non-thermal distribution for gradual events that we see for impulsive events. This is *not* the case.

As the shock in a gradual event passes over an active region, it must average contributions (1) from impulsive suprathermal ions, which have enhancements in Fe/O and ^{3}He/^{4}He, for example, and (2) from ions in the ambient ~3 MK plasma, which have no such enhancements. Ko et al. (2013) found that Fe-rich gradual SEP events were commonly connected to active regions. The result of the two contributions is to reduce the enhancements, as observed, and somewhat reduced distributions in the spread of abundance ratios, more like those in the upper panel of Fig. 5.18.

However, if we really want to reduce the spread of the distributions as seen in gradual events, we need to average over *several* small jets producing impulsive SEP events rather than only one; n events will reduce the spread by a factor of $\sqrt{n}$. It is likely that the number of small impulsive SEP events in an active region increases as the event size decreases, contributing a fairly steady flow of impulsive suprathermal ions; each temporarily contributes to the potential seed population before it diminishes. Based on the increasing number of flares with decreasing size, Parker (1988) proposed that a large number of small nanoflares could actually heat the corona. We need only a small increase in the number of jets producing impulsive SEP events that are too small to resolve as separate events, yet adequate to contribute to the seed population of impulsive suprathermal ions above a solar active region which may be subsequently sampled and averaged by a shock wave. Thus, no single impulsive event determines the seed population for acceleration by the shock wave in a subsequent gradual SEP event.

Many small jets (i.e. nanojets?) could also contribute to the periods of persistent ^{3}He seen by Wiedenbeck et al. (2008), of long-lived and recurrent sources (Bučík et al. 2014, 2015; Chen et al. 2015) and, of course, to the substantial persistent ^{3}He abundances below 1 MeV amu^{-1} in the seed population directly observed at 1 AU upstream (see Fig. 2.7) of the shock wave (e.g. Desai et al. 2003).

Source-plasma temperatures provide a powerful new tool for the comparative study of SEP events.

5.9 Open Questions

This section suggests open questions that might be addressed in future research.

1. What can cause the large non-thermal spread of abundances such as C/He in impulsive SEP events when both He and C should be fully ionized? Does source depth in the corona matter?
2. How well do SEP-derived temperatures correlate with directly observed temperatures near the observer's magnetic footpoint early in a gradual SEP event?
3. How do reservoirs contain particles of all energies with such apparently equal efficiency? How do they attain uniformity of intensities with longitude when the particles upstream of the shock do not? Is diffusion along the turbulent shock a factor?

4. In principle, a shock could accelerate 1-MK plasma at one longitude and 3-MK plasma at another longitude. Is this seen? Is there enough lateral transport in and behind the shock to mix SEPs from these sources late in events?
5. What happens when the energy in SEPs exceeds the energy in B at a shock, especially a quasi-perpendicular shock? Does acceleration cease?
6. Some gradual events show evidence of a component of stripped ions (Reames 2016a). Can we distinguish those that do and those that do not have stripped ions by radius and density of their seed population sources? Is there other evidence of deeper and shallower sources of impulsive suprathermal ions?
7. Spectral knees at shocks have been studied theoretically, but is there a theoretical understanding how the spectrum, *at the shock*, could become a double power-law extending to high energies, rather than an exponential? What parameters control the energy and the change in spectral slope? (There are models that would explain the double power law with diffusive transport.)
8. Measurements by a spacecraft nearer the Sun could improve SEP onset timing by removing the blurring effect of scattering during transport. How does the SEP onset time at 10-s or less resolution compare with X-ray and γ-ray-line onsets, type II burst timing, and local shock measurement? Note that intensities may vary as $\sim r^{-3}$, causing extremely high rates in instruments. To what extent do electron and ion sources differ in gradual SEP events?
9. Discrete ionization states affect the assignment of source-plasma temperatures. $^{12}C^{+5}$ is enhanced but $^{12}C^{+6}$ is not; treating Q as 5.5 is approximate. $A/<Q>$ is not the same as $<A/Q>$. Then there is ^{13}C which is always enhanced. Can we improve the estimates of T?

References

Ackermann, M., et al.: High-energy gamma-ray emission from solar flares: summary of Fermi large area telescope detections and analysis of two M-class flares. Astrophys. J. **787**, 15 (2014)

Afanasiev, A., Battarbee, M., Vainio, R.: Self-consistent Monte Carlo simulations of proton acceleration in coronal shocks: effect of anisotropic pitch-angle scattering of particles. Astron. Astrophys. **584**, 81 (2016)

Ajello, M., et al.: Impulsive and long duration high-energy gamma-ray emission from the very bright 2012 March 7 solar flares. Astrophys. J. **789**, 20 (2014)

Axford, W.I.: Acceleration of cosmic rays by shock waves. Proc. 17th Int. Cosmic Ray Conf. (Paris). **12**, 155 (1981)

Bell, A.R.: The acceleration of cosmic rays in shock fronts. I. Mon. Not. R. Astron. Soc. **182**, 147 (1978a)

Bell, A.R.: The acceleration of cosmic rays in shock fronts. II. Mon. Not. R. Astron. Soc. **182**, 443 (1978b)

Berdichevsky, D.B., Szabo, A., Lepping, R.P., Viñas, A.F., Mariana, F.: Interplanetary fast shocks and associated drivers observed through the 23rd solar minimum by Wind over its first 2.5 years. J. Geophys. Res. **105**, 27289 (2000)

Breneman, H.H., Stone, E.C.: Solar coronal and photospheric abundances from solar energetic particle measurements. Astrophys. J. Lett. **299**, L57 (1985)

Bučík, R., Innes, D.E., Mall, U., Korth, A., Mason, G.M., Gómez-Herrero, R.: Multi-spacecraft observations of recurrent ^{3}He-rich solar energetic particles. Astrophys. J. **786**, 71 (2014)
Bučík, R., Innes, D.E., Chen, N.H., Mason, G.M., Gómez-Herrero, R., Wiedenbeck, M.E.: Long-lived energetic particle source regions on the Sun. J. Phys. Conf. Ser. **642**, 012002 (2015)
Chen, N.H., Bučík, R., Innes, D.E., Mason, G.M.: Case studies of multi-day ^{3}He-rich solar energetic particle periods. Astron. Astrophys. **580**, 16 (2015). doi:10.1051/0004-6361/201525618
Wiedenbeck, M. E, Cohen, C.M.S., Cummings, A.C., de Nolfo, G.A., Leske, R.A., Mewaldt, R.A., Stone, E.C., von Rosenvinge, T.T., Persistent energetic ^{3}He in the inner heliosphere. Proc. 30th Int. Cosmic Ray Conf. (Mérida) 1, 91 (2008)
Daibog, E.I., Stolpovskii, V.G., Kahler, S.W.: Invariance of charged particle time profiles at late stages of scr events from the data of multisatellite observations. Cosm. Res. **41**, 128 (2003)
Desai, M.I., Giacalone, J.: Large gradual solar energetic particle events. Living Rev. Sol. Phys. **13**, 3 (2016). doi:10.1007/s41116-016-0002-5
Desai, M.I., Mason, G.M., Dwyer, J.R., Mazur, J.E., Gold, R.E., Krimigis, S.M., Smith, C.W., Skoug, R.M.: Evidence for a suprathermal seed population of heavy ions accelerated by interplanetary shocks near 1 AU. Astrophys. J. **588**, 1149 (2003)
Desai, M.I., Mason, G.M., Wiedenbeck, M.E., Cohen, C.M.S., Mazur, J.E., Dwyer, J.R., Gold, R.E., Krimigis, S.M., Hu, Q., Smith, C.W., Skoug, R.M.: Spectral properties of heavy ions associated with the passage of interplanetary shocks at 1 AU. Astrophys. J. **661**, 1156 (2004)
DiFabio, R., Guo, Z., Möbius, E., Klecker, B., Kucharek, H., Mason, G.M., Popecki, M.: Energy-dependent charge states and their connection with ion abundances in impulsive solar energetic particle events. Astrophys. J. **687**, 623 (2008)
Ellison, D., Ramaty, R.: Shock acceleration of electrons and ions in solar flares. Astrophys. J. **298**, 400 (1985)
Jones, F.C., Ellison, D.E.: The plasma physics of shock acceleration. Space Sci. Rev. **58**, 259 (1991)
Ko, Y.-K., Tylka, A.J., Ng, C.K., Wang, Y.-M., Dietrich, W.F.: Source regions of the interplanetary magnetic field and variability in heavy-ion elemental composition in gradual solar energetic particle events. Astrophys. J. **776**, 92 (2013)
Lario, D.: Heliospheric energetic particle reservoirs: Ulysses and ACE 175-315 keV electron observations, *Proc. 12th Solar Wind Conf.* AIP Conf. Proc. **1216**, 625 (2010)
Lario, D., Decker, R.B.: The energetic storm particle event of October 20, 1989. Geophys. Res. Lett. **29**, 1393 (2002)
Lee, M.A.: Coupled hydromagnetic wave excitation and ion acceleration at interplanetary traveling shocks. J. Geophys. Res. **88**, 6109 (1983)
Lee, M.A.: Coupled hydromagnetic wave excitation and ion acceleration at an evolving coronal/interplanetary shock. Astrophys. J. Suppl. **158**, 38 (2005)
Lee, M.A., Mewaldt, R.A., Giacalone, J.: Shock acceleration of ions in the heliosphere. Space Sci. Rev. **173**, 247 (2012)
Li, G., Zank, G.P., Rice, W.K.M.: Acceleration and transport of heavy ions at coronal mass ejection-driven shocks. J. Geophys. Res. **110**, 6104 (2005)
Mason, G.M., Ng, C.K., Klecker, B., Green, G.: Impulsive acceleration and scatter-free transport of about 1 MeV per nucleon ions in ^{3}He-rich solar particle events. Astrophys. J. **339**, 529 (1989)
Mazzotta, P., Mazzitelli, G., Colafrancesco, S., Vittorio, N.: Ionization balance for optically thin plasmas: rate coefficients for all atoms and ions of the elements H to Ni. Astron. Astrophys. Suppl. **133**, 403 (1998)
McKibben, R.B.: Azimuthal propagation of low-energy solar-flare protons as observed from spacecraft very widely separated in solar azimuth. J. Geophys. Res. **77**, 3957 (1972)
Melrose, D.B.: Plasma Astrophysics. Gordon and Breach, New York (1980)
Melrose, D.B., Pope, M.H.: Diffusive shock acceleration by multiple shocks. Proc. Astron. Soc. Aust. **10**, 222 (1993)
Mewaldt, R.A., Looper, M.D., Cohen, C.M.S., Haggerty, D.K., Labrador, A.W., Leske, R.A., Mason, G.M., Mazur, J.E., von Rosenvinge, T.T.: Energy spectra, composition, other properties of ground-level events during solar cycle 23. Space Sci. Rev. **171**, 97 (2012)

Ng, C.K., Reames, D.V.: Focused interplanetary transport of approximately 1 MeV solar energetic protons through self-generated Alfven waves. Astrophys. J. **424**, 1032 (1994)
Ng, C.K., Reames, D.V.: Pitch angle diffusion coefficient in an extended quasi-linear theory. Astrophys. J. **453**, 890 (1995)
Ng, C.K., Reames, D.V.: Shock acceleration of solar energetic protons: the first 10 minutes. Astrophys. J. Lett. **686**, L123 (2008)
Ng, C.K., Reames, D.V., Tylka, A.J.: Effect of proton-amplified waves on the evolution of solar energetic particle composition in gradual events. Geophys. Res. Lett. **26**, 2145 (1999)
Ng, C.K., Reames, D.V., Tylka, A.J.: Modeling shock-accelerated solar energetic particles coupled to interplanetary Alfvén waves. Astrophys. J. **591**, 461 (2003)
Ng, C.K., Reames, D.V., Tylka, A.J.: Solar energetic particles: shock acceleration and transport through self-amplified waves. AIP Conf. Proc. **1436**, 212 (2012)
Palmer, I.D.: Transport coefficients of low-energy cosmic rays in interplanetary space. Rev. Geophys. Space Phys. **20**, 335 (1982)
Parker, E.N.: Interplanetary Dynamical Processes. Interscience, New York (1963)
Parker, E.N.: Nanoflares and the solar X-ray corona. Astrophys. J. **330**, 474 (1988)
Post, D.E., Jensen, R.V., Tarter, C.B., Grasberger, W.H., Lokke, W.A.: Steady-state radiative cooling rates for low-density, high temperature plasmas. At. Data Nucl. Data Tables. **20**, 397 (1977)
Reames, D.V.: Acceleration of energetic particles by shock waves from large solar flares. Astrophys. J. Lett. **358**, L63 (1990)
Reames, D.V.: Particle energy spectra at traveling interplanetary shock waves. Astrophys. J. **757**, 93 (2012)
Reames, D.V.: The two sources of solar energetic particles. Space Sci. Rev. **175**, 53 (2013)
Reames, D.V.: Element abundances in solar energetic particles and the solar corona. Sol. Phys. **289**, 977 (2014)
Reames, D.V.: Temperature of the source plasma in gradual solar energetic particle events. Sol. Phys. **291**, 911 (2016a). doi:10.1007/s11207-016-0854-9. arXiv: 1509.08948
Reames, D.V.: The origin of element abundance variations in solar energetic particles. Sol. Phys. **291**, 2099 (2016b). doi:10.1007/s11207-016-0942-x. arXiv: 1603.06233
Reames, D.V., Ng, C.K.: Streaming-limited intensities of solar energetic particles on the intensity plateau. Astrophys. J. **722**, 1286 (2010)
Reames, D.V., Barbier, L.M., von Rosenvinge, T.T., Mason, G.M., Mazur, J.E., Dwyer, J.R.: Energy spectra of ions accelerated in impulsive and gradual solar events. Astrophys. J. **483**, 515 (1997a)
Reames, D.V., Kahler, S.W., Ng, C.K.: Spatial and temporal invariance in the spectra of energetic particles in gradual solar events. Astrophys. J. **491**, 414 (1997b)
Reames, D.V., Ng, C.K., Tylka, A.J.: Initial time dependence of abundances in solar particle events. Astrophys. J. Lett. **531**, L83 (2000)
Reames, D.V., Ng, C.K., Berdichevsky, D.: Angular distributions of solar energetic particles. Atrophys. J. **550**, 1064 (2001)
Rice, W.K.M., Zank, G.P., Li, G.: Particle acceleration and coronal mass ejection driven shocks: shocks of arbitrary strength. J. Geophys. Res. **108**, 1369 (2003)
Roelof, E.C.: Propagation of solar cosmic rays in the interplanetary magnetic field. In: Ögelman, H., Wayland, J.R. (eds.) Lectures in High-Energy Astrophysics. NASA SP-199, Washington, DC (1969)
Roelof, E.C., Gold, R.E., Simnett, G.M., Tappin, S.J., Armstrong, T.P., Lanzerotti, L.J.: Low-energy solar electrons and ions observed at ULYSSES February–April, 1991- The inner heliosphere as a particle reservoir. Geophys. Res. Lett. **19**, 1247 (1992)
Rouillard, A., Sheeley N.R., Jr., Tylka, A., Vourlidas, A., Ng, C.K., Rakowski, C., Cohen, C.M.S., Mewaldt, R.A., Mason, G.M., Reames, D., et al.: The longitudinal properties of a solar energetic particle event investigated using modern solar imaging. Astrophys. J. **752**, 44 (2012)
Ryan, J.M.: Long-duration solar gamma-ray flares. Space Sci. Rev. **93**, 581 (2000)

Sandroos, A., Vainio, R.: Simulation results for heavy ion spectral variability in large gradual solar energetic particle events. Astrophys. J. **662**, L127 (2007)
Stix, T.H.: The Theory of Plasma Waves. McGraw-Hill, New York (1962)
Stix, T.H.: Waves in Plasmas. AIP, New York (1992)
Tan, L.C., Reames, D.V., Ng, C.K., Shao, X., Wang, L.: What causes scatter-free transport of non-relativistic solar electrons? Astrophys. J. **728**, 133 (2011)
Terasawa, T., Oka, M., Nakata, K., Keika, K., Nosé, M., McEntire, R.W., Saito, Y., Mukai, T.: Cosmic-ray-mediated interplanetary shocks in 1994 and 2003. Adv. Space Res. **37**, 1408 (2006)
Vestrand, W.T., Forrest, D.J.: Evidence for a spatially extended component of gamma rays from solar flares. Astrophys. J. Lett. **409**, L69 (1993)
Zank, G.P., Rice, W.K.M., Wu, C.C.: Particle acceleration and coronal mass ejection driven shocks: a theoretical model. J. Geophys. Res. **105**, 25079 (2000)
Zank, G. P., Li, G., Florinski, V., Hu,, Q., Lario,, D., Smith, C. W., Particle acceleration at perpendicular shock waves: model and observations, J. Geophys. Res., 111, A6108 (2006)
Zank, G.P., Li, G., Verkhoglyadova, O.: Particle acceleration at interplanetary shocks. Space Sci. Rev. **130**, 255 (2007)